time–harmonic initial voltage and current $Ve^{-jk_0z'}$ and $Ie^{-jk_0z'}$, and again defining $\Delta z = \tau v$, leads to

$$\begin{bmatrix} V(z) \\ I(z) \end{bmatrix} = \begin{bmatrix} \cos(k_o\Delta z) & jZ_0\sin(k_o\Delta z) \\ \dfrac{j\sin(k_o\Delta z)}{Z_0} & \cos(k_o\Delta z) \end{bmatrix} \begin{bmatrix} Ve^{-jk_oz} \\ Ie^{-jk_oz} \end{bmatrix} \quad (17)$$

The bracketed matrix term in (17) is the well-known time–harmonic two-port transmission-line $ABCD$-parameter matrix. Using this result, it can be reasoned that (15) is the time-domain equivalent to the frequency-domain $ABCD$ matrix (17).

Finally, it is observed that a traditional D'Alembert solution for the coupled system (3) can be extrapolated from (15) by removing those portions of the previous time V and I that do not contribute to the present time $V(z, t)$, $I(z, t)$ as follows:

$$V(z,t) = \frac{\left[V^-(z+tv) + V^+(z-tv)\right]}{2} + \frac{\left[Z_0^-I^-(z+tv) - Z_0^+I^+(z-tv)\right]}{2} \quad (18a)$$

$$I(z,t) = \frac{\left[V^-(z+tv)/Z_0^- - V^+(z-tv)/Z_0^+\right]}{2} + \frac{\left[I^-(z+tv) + I^+(z-tv)\right]}{2}. \quad (18b)$$

It can be easily shown that (18) reduce to (2) by making the substitutions $Z_0^\pm = \pm V^\pm/I^\pm$ in (18) and recognizing that the arguments $t \pm z/v$ and $z \pm tv$ have the same interpretation.

REFERENCES

[1] N. N. Rao, *Elements of Electromagnetic Engineering*, 5th ed. Englewood Cliffs, NJ: Prentice-Hall, 2000.

[2] R. E. Collin, *Foundations for Microwave Engineering*. New York: McGraw-Hill, 1966, sec. 5.12.

[3] P. Pramanick and P. Bhartia, "A generalized theory of tapered transmission line matching transformers and asymmetric couplers supporting non-TEM modes," *IEEE Trans. Microwave Theory Tech.*, vol. 37, pp. 1184–1190, Aug. 1989.

[4] G. Barton, *Elements of Green's Functions and Propagation*. New York: Oxford, 1989.

[5] P. M. DeRusso, R. J. Roy, and C. M. Close, *State Variables for Engineers*. New York: Wiley, 1965.

[6] P. L. E. Uslenghi, "Pulse propagation on lossy lines," in *AMEREM'96 Dig.*, Albuquerque, New Mexico, May 1996, p. 348.

[7] ——, "On the time-domain analysis of transmission lines," in *IEEE AP-S Int. Symp. Dig.*, Atlanta, GA, June 1998, p. 888.

[8] *Libra: A Software Simulator for Microwave and RF Circuits, Version 6.1*. Westlake Village, CA: HP-EEsof, 1999.

Etched-Silicon Micromachined W-Band Waveguides and Horn Antennas

Bassem A. Shenouda, L. Wilson Pearson, and James E. Harriss

***Abstract*—Micromachining of silicon is broadly proposed for the fabrication of substrates and waveguides at millimeter wavelengths. This paper presents the results of the fabrication of finned diamond-shaped waveguides and horn antennas by way of ethylene–diamene–pyrocatechol anisotropic etching of silicon. The structure is fabricated in two halves by etching V grooves in (100) silicon wafers. The etched faces of the wafers were metallized with gold. Metallic fins evaporated on a thin layer of Mylar and sandwiched between the two halves of the structure were used to improve the bandwidth of the waveguide. Measurements were taken of the dispersion curve of the waveguide with fins with different gap separations, and of the radiation patterns of the fabricated horns with different flare angles at different frequencies. Measurements showed a very good agreement with numerical calculations using the finite-element-method technique. Computed attenuation curves for the structure are provided as well.**

***Index Terms*—Horn antennas, micromachining, millimeter wave antennas.**

I. INTRODUCTION

Silicon micromachining has been used to fabricate millimeter-wave horn antennas and waveguides [1]–[3]. The flare angle of the previously reported fabricated antennas [1], [2] was limited to 70.52° by the (111) silicon crystal planes. To overcome the angle limitation, Guo [2] and Johansson and Whyborn [4] suggested a diamond-shaped horn antenna etched in silicon, and its fabrication was first reported by the authors [5]. Crowe *et al.* reported the fabrication of receivers and mixers using a similar horn structure [6], [7]. This structure can be fabricated with different horn flare angles, which is desirable from a design point-of-view. A diamond-shaped structure arises naturally through wet-etch micromachining of a (100) silicon wafer. The waveguide walls are aligned with the (111) crystal planes, and the flare of the horns is a fine-scale corrugation of triangular cross sections, all characterized by the 70.52° angle between the (111) planes. However, since the etching process is anisotropic and the etch in the (100) direction is dominant, the final shape approximates the shape of the mask, but is corrupted to a small extent by etching in directions other than the (100) direction. Optical measurements are used to determine the actual flare angle of the fabricated structure and the dimensions of the horn opening. The measured dimensions are used in the numerical calculations.

II. FABRICATION

The antenna/waveguide assemblies depicted in Fig. 1(a) were formed by etching 3-mm-thick (100) silicon wafers using ethylene–diamene–pyrocatechol (EDP) etchant solution indicated by Wu *et al.* [8]. The wafer was masked with a pattern consisting of three pairs of waveguide/horn structures to fabricate three waveguide/horn assemblies with different horn-flare angles. The masked wafer was etched with agitation in the EDP solution at a temperature of 110 °C

Manuscript received December 15, 1999; revised May 12, 2000. This work was supported by the U.S. Federal Aviation Administration under Grant 93-G-047.

The authors are with the Holcombe Department of Electrical and Computer Engineering, Clemson University, Clemson, SC 29634-0915 USA (e-mail: bshenou@ces.clemson.edu; pearson@ces.clemson.edu; james.harriss@ces.clemson.edu).

Publisher Item Identifier S 0018-9480(01)02443-7.

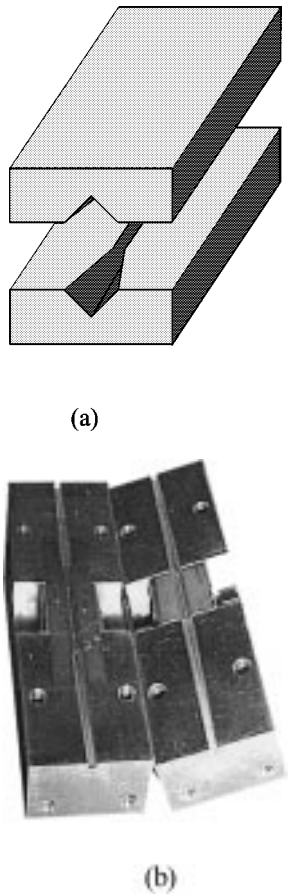

Fig. 1. (a) Cross section of diamond-shaped waveguide/horn "clamshells" formed from etched V grooves in (100) silicon wafer. (b) Measurement jig with metallized clamshells in place. The jig provides a transition from rectangular to diamond cross section. The film on which the fin metallization is suspended is barely visible on the left-hand-side half.

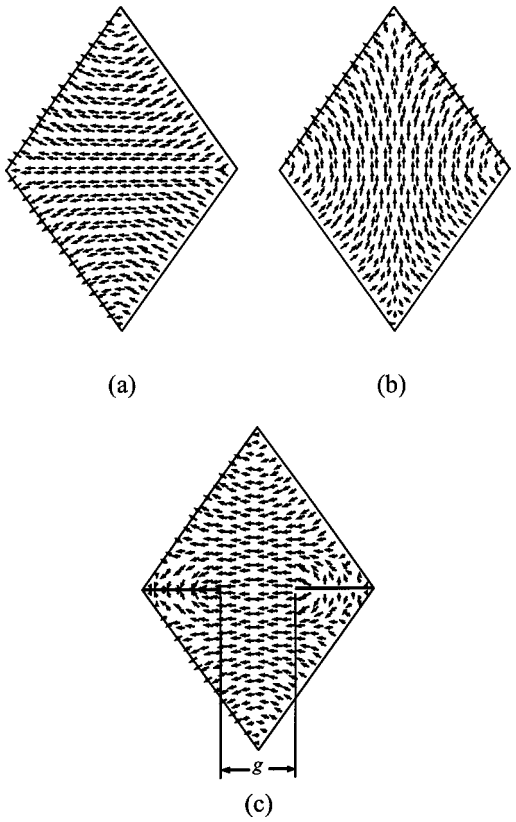

Fig. 2. Electric-field intensity representation for: (a) first and (b) second propagating modes in diamond-shaped waveguide. Modification of the field pattern for the first mode in the presence of fins is shown in (c). Since the field lines of the second mode are normal to the fins, this mode is unaffected by the presence of the fin.

for the time needed to produce the desired depth at the deepest point inside the horn (2.5 mm in 25 h). The width of the channels in the mask is slightly less than the desired width of the final fabricated structure to compensate for the etch in the (111) direction (2 μm/h). Sawing the etched wafer along thin scribe lines freed the horn/waveguide pairs. Each antenna was then formed by sawing the etched wafer at the horn and waveguide openings, and folding the halves together in clamshell fashion. The different horns were cut to have the same length, thus, the horn with bigger flare angles would have bigger aperture areas. The diagonals of the openings of the fabricated waveguides for W-band operation were 1.92 and 2.72 mm, with the shorter length along the interface between the two halves. The structure was coated with gold in a thermal evaporator to give a thin conducting layer. A layer of gold of approximately six times the skin depth at the operating frequency (6×0.25 μm) was then electroplated onto the structure. Aluminum fins were formed on a thin Mylar membrane that was sandwiched between the two halves of the structure. The wafer thickness limits the size of the aperture realized. The work reported here was done to investigate the concept of etching flare angles that are not restricted to the angles of the crystal planes. Thicker wafers obviously can be used to achieve larger horn apertures.

III. Measurement Jig

Brass waveguides were machined to provide a smooth transition from the micromachined diamond-shaped waveguide to the standard rectangular waveguide used in the measurements. Fig. 1(b) shows two pairs of jigs with the metallized micromachined waveguide in place. The metallic fins were tapered inside the brass waveguide to minimize reflection. This setting was used for the dispersion curve measurements of the waveguide. The silicon waveguide is deembedded from the measurement by performing the S_{21} reference calibration with the two transition sections of the jig in direct contact with each other. The propagation constant β is determined from the measured phase difference and the length of the silicon waveguide. For the radiation pattern measurements, only one pair of jigs was used and the micromachined waveguide was replaced by the waveguide/horn assembly. The metallic fins were tapered inside the horn.

IV. Modeling and Results

We performed numerical calculations using the finite-element method (FEM) technique with edge-based vector basis functions to determine the cutoff frequencies of the waveguide and field distribution for each propagating mode. In the traditional fashion, the cutoff wavenumbers are the eigenvalues of the FEM system and the modal field distribution results form the associated eigenvectors. Fig. 2 shows the field distribution of the first two propagating modes in a diamond-shaped waveguide and the first mode in a finned waveguide. The first two modes for the diamond-shaped waveguide correspond to the TE_{10} and TE_{01} modes in a rectangular waveguide. It is noted that the field lines of the second mode are perpendicular to the horizontal plane—the plane in which fins are to be placed. Consequently, the conducting fins will have no effect on this mode. On the other hand, the first propagating mode, with strong field component parallel to the plane of fins, will be strongly influenced by the presence of fins. The

TABLE I
LOWEST VALUES OF CUTOFF FREQUENCY FOR THE WAVEGUIDE AS A FUNCTION OF g

N	No fins	g=1.22 mm	g=0.82 mm	g=0.64 mm
1	80.28 GHz TE	77.69 GHz TE	70.14 GHz TE	64.52 GHz TE
2	106.4 GHz TE	106.4 GHz TE	106.4 GHz TE	106.4 GHz TE
3	123.5 GHz TE	123.5 GHz TE	123.5 GHz TE	119.3GHz TE
4	133.5 GHz TM	137.8 GHz TM	129.4 GHz TE	123.5 GHz TE
5	183 GHz TE	162.5 GHz TE	141 GHz TE	134.3 GHz TE

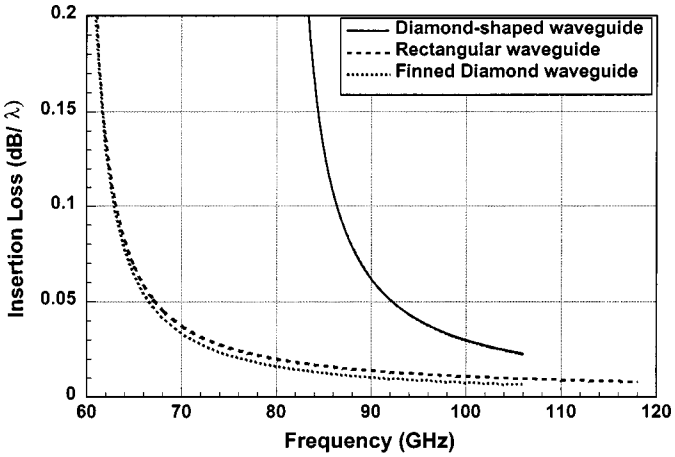

Fig. 3. Calculated insertion loss for W-band rectangular and diamond-shaped waveguides.

cutoff frequencies of the finned diamond-shaped waveguide are given in Table I for the first five modes and for different fin separations g.

The cutoff frequency for the first mode decreases as the gap between the fins decreases, while the cutoff frequency for the second mode is unaffected by the fins. (The reason for this is clear from Fig. 2(b), where field lines for the second mode are transversely oriented at the fin sites.) Thus, the single-mode bandwidth of the guide can be adjusted by means of the fin separation. Fig. 3 displays the attenuation of several W-band waveguides as a function of frequency. The solid curve shows the attenuation of a diamond cross-sectional waveguide of the dimensions given in Section II. The attenuation of a standard gold WR-10 waveguide is shown with a dashed line. The third curve in the figure is the attenuation of the diamond cross-sectional guide with fins added so that the cutoff frequency of the dominant mode is 59 GHz, the same cutoff as WR-10 waveguide. It is seen that the attenuation curves for the finned diamond guide and for WR-10 are virtually identical. We have made a number of additional attenuation calculations that reveal that any variant of the diamond waveguide exhibits attenuation comparable with that of WR-10 as long as the dominant-mode cutoff frequencies of the two guides agree. Variations in the conductivity of the fins and in the cutoff frequency for the second propagating mode affect the attenuation only weakly.

V. MEASUREMENTS

Finned waveguides have been fabricated for a number of fin separations. Dispersion curves have been measured for these waveguides and compared with the calculated dispersion curves. These results are shown in Fig. 4. One can infer from these curves, errors in cutoff frequency ranging from 1% to 3%. The radiation patterns were taken of the horns with different flare angles at 94 GHz. The angles of the fabricated horns were measured and found to be equal to 8.5°, 17°, and

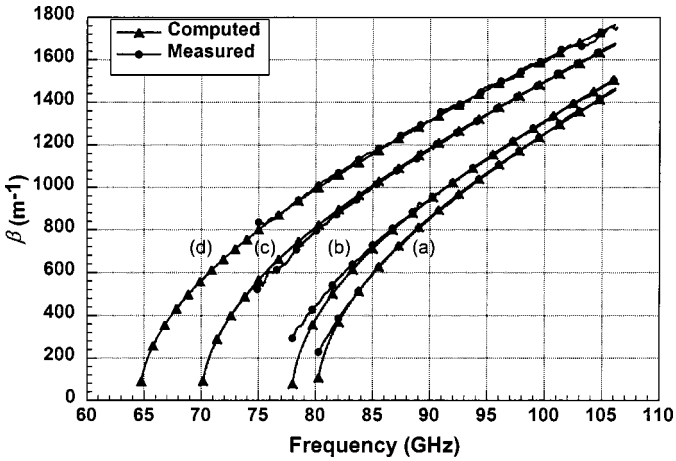

Fig. 4. Measured and computed dispersion curves for the dominant mode in the finned diamond guide for four fin separations: (a) no fins, (b) $g = 1.22$ mm, (c) $g = 0.82$ mm, and (d) $g = 0.64$ mm.

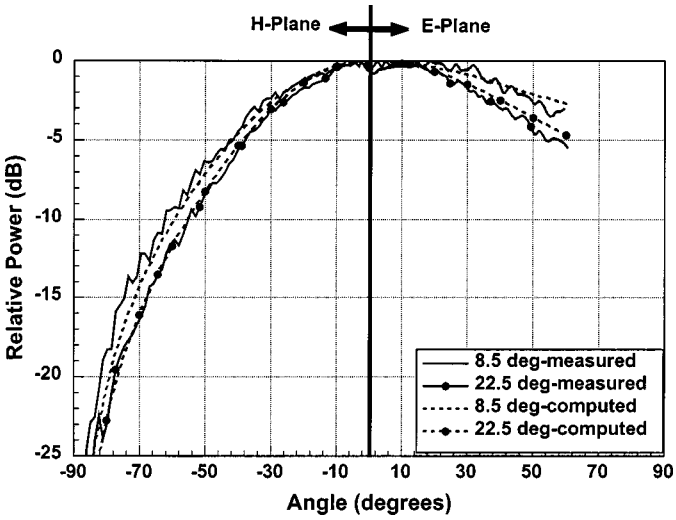

Fig. 5. Measured radiation patterns at 94 GHz of two different horns with flare angles of 8.5° and 22.5°. The E-plane radiation pattern measurement stops at 60 because of mechanical constraints in antenna/absorber arrangement used in performing the measurements.

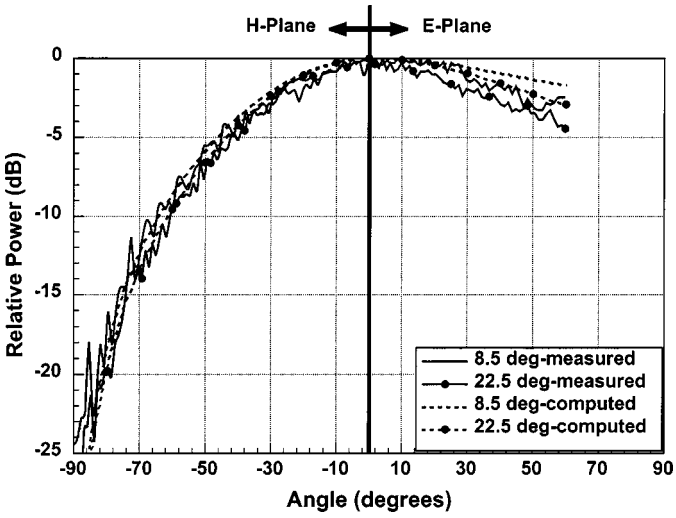

Fig. 6. Measured radiation patterns at 75 GHz of two different horns with flare angles of 8.5° and 22.5°. Fins with a gap separation of 0.6 mm were used to lower the cutoff frequency of the waveguide.

22.5°. Tapered fins, with a gap separation of 0.6 mm in the waveguide, were used to make radiation pattern measurements at 75 GHz. E- and H-plane radiation patterns of these measurements are shown in Figs. 5 and 6, along with calculated patterns. We conclude from these figures that the radiation patterns get narrower for the horn with the big flare angle, which corresponds to a big aperture area. We can also see that the patterns measured at 94 GHz are narrower than the ones measured at 75 GHz, which is expected since the electrical dimensions of the aperture become relatively large compared to the wavelength at higher frequencies. From our measurements of the radiation patterns of the finned structure at 94 GHz, we concluded that using the fins lowered the cutoff frequency of the waveguide without any significant effect on the radiation patterns. The comparison between the measured and calculated patterns shows, in general, a good agreement.

VI. Conclusions

W-band micromachined waveguides and horn antennas were fabricated using EDP anisotropic etching of silicon. Measurements of the dispersion curves were taken for finned waveguides with different fin separations. These measurements were compared to those calculated using the FEM technique, and the comparison showed a good agreement with an error in cutoff frequency of less than 3%. Radiation pattern measurements of horns were taken at 94 GHz before using the fins, then at 75 and 94 GHz after using fins in the structure to lower the cutoff frequency of the waveguide. Comparison between the measured and calculated patterns showed a good agreement. The fin structure can be transitioned into the coplanar waveguide for integration with monolithic system components.

Acknowledgment

The authors wish to express their gratitude to Dr. Yong Guo, TRW Inc., Redondo Beach, CA, for his collaboration in the formative stages of this paper.

References

[1] G. M. Rebeiz, D. P. Kasilingam, Y. Guo, P. A. Stimson, and D. B. Rutledge, "Monolithic millimeter-wave two-dimensional horn imaging arrays," *IEEE Trans. Antennas Propagat.*, vol. 38, pp. 1473–1482, Sept. 1990.

[2] Y. Guo, "Millimeter-wave integrated-circuit horn-antenna imaging arrays," Ph.D. dissertation, Dept. Elect. Eng., California Inst. Technol., Pasadena, CA, 1991.

[3] M. Yap, Y. Tai, W. R. McGrath, and C. Walker, "Silicon micromachined waveguides for millimeter and submillimeter wavelengths," in *Proc. IEEE 3rd Int. Space Terahertz Technol. Symp.*, Ann Arbor, MI, Mar. 1992, pp. 316–323.

[4] J. K. Johansson and N. D. Whyborn, "The diagonal horn as a sub-millimeter wave antenna," *IEEE Trans. Microwave Theory Tech.*, vol. 40, pp. 795–800, May 1992.

[5] B. Shenouda, L. W. Pearson, J. E. Harriss, W. Wang, and Y. Guo, "Etched-silicon micromachined waveguides and horn antennas at 94 GHz," in *IEEE AP-S Int. Symp. Dig* , Baltimore, MD, 1996, pp. 988–991.

[6] T. W. Crowe, P. J. Koh, W. L. Bishop, C. M. Mann, J. L. Hesler, R. M. Weikle, P. A. D. Wood, and D. Matheson, "Inexpensive receiver components for millimeter and submillimeter wavelengths," in *Proc. IEEE 8th Int. Space Terahertz Technol. Symp.*, Cambridge, MA, Mar. 1997, pp. 377–384.

[7] T. W. Crowe, J. L. Hesler, R. M. Weikle, and S. H. Jones, "GaAs devices and circuits for terahertz applications," *Infrared Phys. Technol.*, vol. 40, pp. 175–189, 1999.

[8] X. Wu, Q. Wu, and W. H. Ko, "A study on deep etching of silicon using ethylene–diamine–pyrocatechol–water," *Sens. Actuators*, vol. 9, pp. 333–343, 1986.

Improved Design of Broad-Band Latching Ferrite Phase Shifter in a Reduced-Size Grooved Waveguide

Wenquan Che, Edward Kai-Ning Yung, Wen Junding, and Kan Sha

***Abstract*—In this paper, an improved design of a broad-band latching ferrite phase shifter in grooved waveguide is discussed. The elimination technique for the insertion-loss peak is also introduced. The little gaps between the metal bars and waveguide wall are beneficial to suppress the high-order modes caused by the filling of high constant dielectric in the ferrite toroid. The theoretical and measured results have shown that the changes in differential phase shift with frequency remains less than 2.2%; the insertion loss and voltage standing-wave ratio of the device are good over the band 2∼4 GHz.**

***Index Terms*—Broad-band phase shifter, ferrite, grooved waveguide.**

I. Introduction

The development of a phased-array electronic-warfare system requires that the ferrite phase shifters have improved performance, such as shorter switch time, higher figure-of-merit, higher power-handling capacity, as well as broader bandwidth. Though the fluctuation of insertion loss and voltage standing-wave ratio (VSWR) for broad-band ferrite phase shifters are not critical in the system, many problems have existed in the design of the broad-band ferrite phase shifter [1], [2]. For example, there have been severe fluctuations of the insertion loss and a big slope of phase shift with frequency. In this paper, we present an improved design of the broad-band latching ferrite phase shifter in reduced-size grooved waveguide. Suitable selection of geometrical dimension and ridge height can result in smoother differential phase shift versus frequency; the little gaps existed in the innovative grooved waveguide are beneficial to suppress the high-order modes, which caused high loss peak. Furthermore, the coaxial-waveguide impedance-matching structure filled with dielectric can help to obtain good VSWR characteristic over the broad band. The experimental and theoretical results all show that, compared with the broad-band ferrite phase shifter in rectangular waveguide, the insertion loss of the ferrite phase shifter in grooved waveguide is decreased by 10%∼20%, differential phase shift is increased by 20%∼30%, the peak power capacity is improved by 10%, and the average power capacity is improved by 40%∼50%.

II. Design Considerations

A. Consideration of Differential Phase Shift Versus Frequency

1) Choice of Waveguide Structure: As we all know, the advantages of the ferrite phase shifter in grooved waveguide [3]–[6] are large differential phase shift, small insertion loss, and high power-handling capacity. However, there has been no literature on the broad-band ferrite phase shifter in grooved waveguide because the slope of the differen-

Manuscript received December 21, 1999; revised May 15, 2000. This work was supported by the Competitive Earmarked Research Grant, Research Grant Council, Hong Kong Special Administrative Region.

W. Che is with the Department of Electronic Engineering, City University of Hong Kong, Kowloon, Hong Kong and is also with the Department of Electrical Engineering, Nanjing University of Science and Technology, 210094 Nanjing, China.

E. K.-N. Yung is with the Department of Electronic Engineering, City University of Hong Kong, Kowloon, Hong Kong.

W. Junding and K. Sha are with the Department of Electrical Engineering, Nanjing University of Science and Technology, 210094 Nanjing, China.

Publisher Item Identifier S 0018-9480(01)02424-3.